

The Two Components of the Crystallographic Transition in VO₂*

JOHN B. GOODENOUGH

Lincoln Laboratory, Massachusetts Institute of Technology, Lexington, Massachusetts 02173

Received March 15, 1971

Two distinguishable mechanisms of the monoclinic-to-tetragonal transition in VO₂ are identified: an antiferroelectric-to-paraelectric transition at a temperature T_t , as well as a change from homopolar to metallic V-V bonding at a temperature T_t' . In pure VO₂ at atmospheric pressure, the two transitions occur at the same temperature, $T_t' = T_t = 340^\circ\text{K}$. However, a $T_t' < T_t$ may be induced by atomic substitutions; and in the intermediate temperature range the structure is orthorhombic, the antiferroelectric distortions being somewhat different in the absence of homopolar V-V bonding. From energy-band considerations, the semiconductor-to-metal transition is to be associated with the transition at T_t ; but below T_t' the semiconducting energy gap should be larger and the charge-carrier mobilities should be smaller. The existence of two transition temperatures in doped VO₂ is distinguished from the claim of two transition temperatures in the Magnéli phases V_nO_{2n-1}. In this latter case, the appearance of two transitions reflects a two-phase region consisting of two adjoining Magnéli phases.

I. Introduction

Over a decade ago, Morin (1) reported a first-order semiconductor-to-metal transition in VO₂ at a transition temperature $T_t \approx 340^\circ\text{K}$. In his sample, the electrical discontinuity across the transition was about two orders of magnitude. Subsequently discontinuities as large as five orders of magnitude have been observed (2). In these latter, apparently more stoichiometric, samples the thermal hysteresis associated with the transition is sharply reduced ($\Delta T_t \approx 1^\circ\text{K}$), but the T_t obtained with increasing temperature remains essentially unchanged.

High-temperature VO₂ has the tetragonal ($P4_2/mnm$) rutile structure illustrated in Fig. 1; low-temperature VO₂ has the monoclinic ($P2_1/c$) structure of Fig. 2. A striking feature of this monoclinic phase is the presence of cation-cation pairs along the $a_m = 2c_r$ axis, alternate V-V separations being 2.65 and 3.12 Å in place of the regular 2.87 Å spacing in the tetragonal phase just above T_t . This feature immediately suggests metal-metal bonding (3, 4), and the conditions for a transition from cation clustering to the formation of narrow, cation-sublattice d bands were argued (5) and shown to be satisfied by VO₂ (6). Alder and Brooks (7) developed the model further, introducing the idea that an

energy gap produced by cation clustering would decrease with n , the number of electrons excited from intracluster bonding to intracluster anti-bonding states. They were able to show that, in the absence of electron correlations, this model accounts for a first-order transition at T_t and gives a

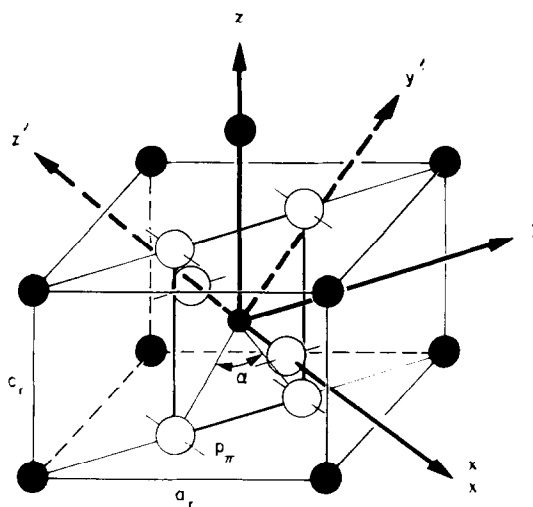


FIG. 1. Tetragonal, rutile structure, space group $P4_2/mnm$. Open circles O²⁻ with orientation of p_π orbitals, closed circles V⁴⁺.

* This work was sponsored by the Department of the Air Force.

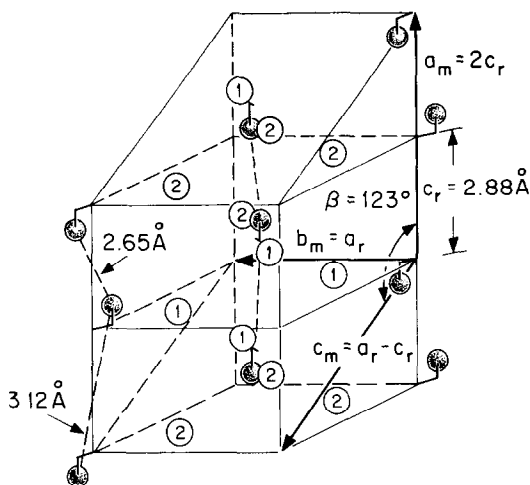


FIG. 2. Monoclinic $P2_1/c$ structure of low-temperature VO₂ and its relationship to the rutile structure.

quantitative relationship between T_t and the energy gap E_{g0} at $T = 0^\circ\text{K}$, where $n = 0$:

$$E_{g0}/kT_t = 8.10. \quad (1)$$

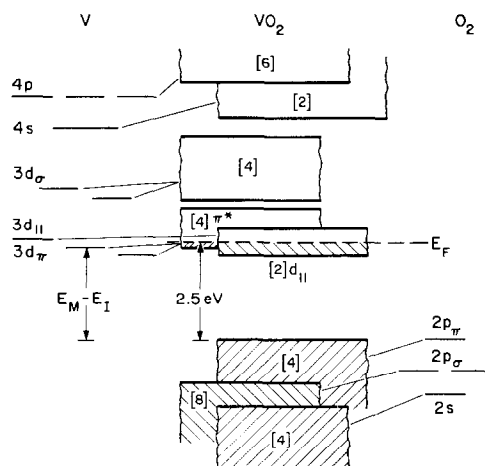
Although the energies $q = d(\ln\rho)/d(kT)^{-1}$ from conductivity data increase from 0.15 eV at lowest temperatures to 0.5 eV just below T_t (8, 9), optical data (2, 10) indicate that the energy gap opened up in the d bands by the distortion is $E_{g0} \approx 0.8$ eV, which is too large relative to $T_t = 340^\circ\text{K}$ to satisfy Eq. (1). More seriously, Berglund and Jayaraman (11) have shown that, although the transition temperature increases with hydrostatic pressure ($dT_t/dP > 0$), nevertheless $dE_g/dP < 0$. This latter fact seems to eliminate cation clustering as the driving mechanism responsible for the transition at T_t . Furthermore, there is little reason to expect that a simple one-band theory can be adequate for VO₂.

Heckingbottom and Linett (12) were the first to emphasize the second significant feature of the low-temperature structure (Fig. 2): a tilting of c_r -axis, V-V pairs to give one shortest vanadium-oxygen ($V-O_1$) separation $R_{VO} = 1.76$ Å perpendicular to the c_r axis. The two bridging oxygens O_{11} between paired vanadium ions have $R_{VO} = 1.86, 1.87$ Å. The other three cation-anion distances are $R_{VO} = 2.01, 2.03,$ and 2.05 Å. The displacement of a cation from the center of its interstice toward one or more anions is characteristic of a ferroelectric-type distortion, and this feature of the low-temperature structure suggests that an antiferroelectric distortion coincides with the formation of V-V homopolar bonds below T_t . Thus the driving mechanism responsible for the transition at T_t may be an anti-

ferroelectric transition. It is this idea that is explored in this paper.

II. Band Structure for Tetragonal VO₂

Construction of an energy-level diagram for VO₂ begins with the observation that the electrostatic Madelung energy E_M for the effective charges on the ions is able to stabilize the $O^{2-}:2p$ orbitals relative to the $V^{4+}:3d$ orbitals, even after the ionization energy of the cation and electron affinity of the anion are taken into account to reduce the stabilization energy to $(E_M - E_I)$. Figure 3 shows schematically the one-electron $3d, 4s, 4p$ energy levels for ionic V^{4+} at the left, the $2s, 2p$ energy levels for ionic O^{2-} at the right. Crystal-field splittings of the $3d$ and $2p$ levels are also indicated. From Fig. 1, each anion has three, coplanar near-neighbor cations, and the anion p_π orbitals are directed perpendicular to this plane. The cubic component of the V^{4+} -ion octahedral sites splits the $3d^1$ energies into less-stable, twofold-degenerate states of E_g symmetry and more-stable threefold-degenerate states of T_{2g} symmetry. The occupied octahedral sites share common edges only along the c_r axis, so that an orthorhombic component of the crystalline field is present to completely remove the d -state degeneracies. The two e_g orbitals are split into two d_σ orbitals and the three t_{2g} orbitals into two d_π orbitals, which mix with the anion p_π orbital, and a d_\parallel orbital directed along the c_r axis.



SCHMATIC ENERGY BANDS for TETRAGONAL VO₂

FIG. 3. One-electron band structure for tetragonal VO₂.

The outer s and p electrons, which are primarily responsible for the binding energy of the crystal, must be treated by an itinerant-electron model. At the center of the Brillouin zone, the $2s2p\sigma^2$ orbitals at the two anions per cation σ -bond with the cation $3d\sigma^24s4p\sigma^3$ orbitals to form cation-anion bonding and antibonding orbitals. Covalent mixing destabilizes the antibonding, primarily cationic orbitals and stabilizes the bonding, primarily anionic orbitals. Covalent mixing between O^{2-} ions and $3d\sigma$ orbitals at ions with formal valence M^{4+} is also strong enough to delocalize the $3d\sigma$ orbitals (13), so that these must also be described by an itinerant-electron (band) model. Thus the bonding σ and antibonding σ^* bands of Fig. 3 are generated.

In general, outer $3d$ electrons in oxides may be either itinerant or localized, depending upon the strength of the interactions between $3d$ electrons on neighboring atoms. A measure of the strength of this interaction is the transfer energy

$$b = (\psi_i, \mathcal{H}' \psi_j) \approx \epsilon(\psi_i, \psi_j), \quad (2)$$

where \mathcal{H}' is the perturbation of the potential at \mathbf{R}_j due to the presence of a near-neighbor cation at \mathbf{R}_i , and ϵ is a one-electron energy. The $3d$ orbitals ψ_i and ψ_j are crystal-field orbitals, which contain the admixture of near-neighbor anion orbitals via covalent mixing.

From the orthorhombic axes x, y, z of Fig. 1, the five d orbitals are:

$$\begin{aligned} \psi(a_1) &\approx f_{z^2-y^2}, \\ \psi(b_1) &= N_\pi(f_{xy} - \lambda_\pi \phi_\pi), \\ \psi(b_2) &= N'_\pi(f_{zx} - \lambda'_\pi \phi'_\pi), \\ \psi(a_1') &= N'_\sigma(f_{3x^2-r^2} - \lambda'_s \phi'_s - \lambda'_\sigma \phi'_\sigma), \\ \psi(b_3) &= N_\sigma(f_{yz} - \lambda_s \phi_s - \lambda_\sigma \phi_\sigma), \end{aligned} \quad (3)$$

where the N_i are normalization constants, the f_i are atomic orbitals having the angular dependences shown, the λ_i are covalent-mixing parameters, and the ϕ_i are properly symmetrized, anion s and p orbitals. Because the bridging O^{2-} ions along the c_r axis make $O-V-O$ angles $\alpha < 90^\circ$, there is some σ -bond covalent mixing in $\psi(a_1)$ that is not shown. The first three orbitals correspond to the t_{2g} orbitals of cubic symmetry, the last two to the e_g orbitals. By geometry $\lambda_\sigma > \lambda_\pi$, and the d_σ orbitals $\psi(a_1')$, $\psi(b_3)$ are destabilized by covalent mixing to a larger extent than the d_π orbitals $\psi(b_1)$, $\psi(b_2)$. The relative energies of the $d_{||} = \psi(a_1)$ and d_π orbitals depends upon the c_r/a_r ratio. Whether the $3d_\sigma \sigma^*$ bands overlap the $3d_\pi \pi^*$ bands, or are discrete as shown in Fig. 3, depends upon the relative strengths of λ_s

and λ_π . In a tight-binding approximation, the bandwidths due to cation-anion-cation interactions are

$$W_\sigma \sim b_\sigma \sim \epsilon_\sigma N_\sigma^2 \lambda_\sigma^2, \quad (4)$$

$$W_\pi \sim b_\pi \sim \epsilon_\pi N_\pi^2 \lambda_\pi^2,$$

since the overlap integrals are $(\psi_i, \psi_j) \sim N^2 \lambda^2$.

From studies of the ABO_3 oxides with perovskite structure, it is known that $CaVO_3$ and $SrVO_3$ are metallic and Pauli paramagnetic, characteristic of itinerant $3d_\pi$ electrons (13). This shows that $V^{4+}-O^{2-}:p_\pi - V^{4+}$ interactions have a large enough b_π to require an itinerant-electron description. The large A cations compete for the p_π electrons in the perovskite structure (14), thereby reducing b_π , whereas in VO_2 there is no such competition. Therefore, we must conclude that covalent mixing between the single p_π orbital per anion and the two $3d_\pi$ orbitals per V^{4+} ion results in the formation of narrow, cation-anion-cation antibonding π^* bands as well as broader, bonding π bands.

The remaining $3d$ orbital per V^{4+} ion is essentially nonbonding with respect to the anion array and is directed parallel to the c_r axis. For these orbitals the transfer energy $b = b(R)$ varies sensitively with the V-V separation R along the c_r axis. From studies of several isostructural series of compounds, I have obtained a semiempirical expression for the room-temperature critical separation R_c for localized vs itinerant $3d$ electrons in oxides (6). For a V^{4+} ion, this separation is

$$R_c(V^{4+}) \approx 2.94 \text{ \AA}. \quad (5)$$

Although each vanadium ion has only two nearest neighbors, which would tend to reduce R_c , nevertheless 2.94 \AA is sufficiently larger than the observed $R = 2.88 \text{ \AA}$ that narrow, cation-sublattice $3d_{||}$ itinerant-electron orbitals may be anticipated. However, R is close enough to R_c that electron correlations and strong electron-lattice interactions cannot be ignored.

The relative stabilities of the $d_{||}$ and π^* bands depend upon the crystallographic c_r/a_r ratio. Thermal-expansion data (15) shows that the axial ratio $c_r/a_r \approx 0.626$ at 78°C increases to 0.630 at 415°C . The anisotropy in the thermal expansion coefficients of VO_2 is much greater than that in other oxides with the rutile structure. Since the ideal ionic ratio is $c_r/a_r \approx 0.66$ and $c_r/a_r = 0.64$ in TiO_2 , where no metal-metal bonding is possible, the observed ratios indicate that partially filled $d_{||}$ orbitals provide a cation-cation c_r -axis binding that reduces c_r/a_r , and the stability of the $d_{||}$ band

increases relative to the π^* band with decreasing temperature. Israelsson and Kihlberg (16) have demonstrated the sensitivity of the c_r/a_r ratio to metal-metal bonding along c_r in the $V_{1-x}W_xO_2$ system, which exhibits a maximum $c_r/a_r = 0.64$ at $x = 0.33$, where the V^{3+} and W^{6+} ions order to form the trirutile structure. On the other hand, a nearly isotropic resistivity in metallic VO₂ (17, 18) seems to signal the presence of π^* electrons having larger mobilities than the $d_{||}$ electrons. Since any splitting by the orthorhombic component of the crystalline field should be small relative to the bandwidths, an overlapping of the π^* and $d_{||}$ bands as shown in Fig. 3 is not unexpected. With 17 outer electrons per VO₂ molecule, the Fermi energy would fall where the $d_{||}$ and π^* bands contain, between them, one occupied state per vanadium ion. This is the meaning of a formal valence state V^{4+} .

Placement of the Fermi energy relative to the edge of the π band can be obtained from optical reflectance measurements. The reflectance spectrum gives a typical plasma cutoff at a plasma frequency ω_p corresponding to $\hbar\omega_p \approx 1$ eV (8). This, together with a Hall $n_{eff} \approx 3 \times 10^{20}$ electrons/cm³, gives an optical $m^* \approx 0.5m_e$ and an optical mobility $\mu_{opt} \approx 2$ cm²/V-sec, characteristic of very narrow d bands. The imaginary part of the dielectric constant shows two absorption peaks at ca. 2.8 and 3.6 eV (10). Comparison of these peaks with similar (but of larger amplitude) peaks reported (19) for TiO₂ permits identification of the loss mechanism as $\pi \rightarrow (t_{||}, \pi^*)$ interband transitions, and the π to $(t_{||}, \pi^*)$ band gap is estimated to be $E_g \approx 2.5$ eV. This is to be compared with an $E_g \approx 3.05$ eV in TiO₂. Since vanadium is the next element to the right of titanium in the periodic table, such a relative stabilization of the d bands is to be expected (20). The optical data also provide evidence of two overlapping, partially occupied d bands, which is consistent with an E_F cutting overlapping π^* and $d_{||}$ bands. Photoemission measurements (21) support an energy separation of 2.5 eV between E_F and the top of the π band.

The paramagnetic susceptibility for $T > T_t$ is large for Pauli paramagnetism and exhibits some temperature dependence (22), indicating considerable exchange enhancement. Since the perovskites CaVO₃ and SrVO₃ do not exhibit a similar exchange enhancement, this phenomenon apparently signals the presence of narrow $d_{||}$ bands. This is consistent with an R approaching R_c , since this is the condition for itinerant electrons having strong electron correlations and electron-lattice interactions.

An important feature of Fig. 3 is the existence of overlapping, partially filled, nondegenerate bands. This eliminates any one-band model for the semiconductor-to-metal transition in VO₂.

III. Modifications of the Band Structure at $T < T_t$

Given the band structure of Fig. 3, a transition from a metallic to a semiconducting state requires two distinguishable changes in the band structure: (1) a raising of the π^* bands above the Fermi energy E_F , thus leaving the $d_{||}$ band half-filled, and (2) a splitting of the $d_{||}$ band. Such a change in the d bands is illustrated by Fig. 4.

Raising of the π^* bands above E_F requires either a destabilization of the π^* bands or a stabilization of at least the bottom half of the $d_{||}$ band or both. Destabilization of the π^* bands would result from a crystallographic distortion that increases the splitting between the π and π^* bands; stabilization of the $d_{||}$ bands would be induced by a decrease in the axial ratio c_r/a_r , and the bottom half of the $d_{||}$ band would be stabilized by a doubling of the c_r axis, either through a crystallographic distortion or magnetic ordering, since such a doubling of the c_r axis would split the $d_{||}$ band in two (5, 6). Homopolar V-V bonding along the c_r axis, as I originally suggested (4), would give the required doubling of the c_r axis to split the $d_{||}$ band in two and lower E_F below the bottom of the π^* band. This suggestion is consistent not only with the observed V-V pairing along the c_r axis, but also with the lack of any antiferromagnetic ordering below T_t , as demonstrated by NMR (23) and the Mossbauer effect (24). However, this mechanism does not seem to be the driving force for the transition in VO₂, as pointed out in the Introduction.

Displacement of a V^{4+} ion from the center of symmetry of an octahedral interstice to form one or more shorter V-O bonds occurs commonly in

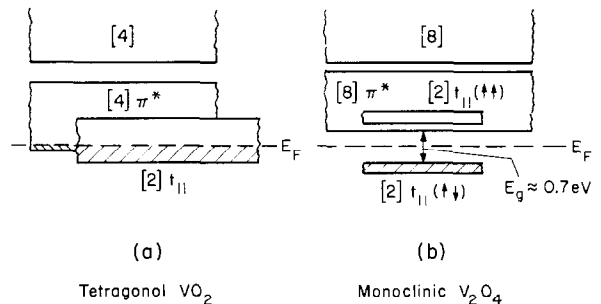


FIG. 4. Schematic modification of d -band structure of VO₂ on passing from metallic to semiconducting phase.

higher valence vanadium oxides. Such a displacement is invariably associated with the availability of anion p_π orbitals for bonding with empty cation d_π orbitals. From structure refinements of the $M_x^+V_2O_5$ - β phases (25, 26) and of V_6O_{13} (27), I have argued (28, 29) that V-O²⁻ separations $R \lesssim 1.60$ Å signal the presence of a double V-O π bond in addition to the σ bonding, whereas V-O separations $\gtrsim 1.89$ Å signal only σ bonding. A V-O separation $1.75 < R_{VO} < 1.81$ Å is characteristic of a single V-O π bond in addition to the σ bonding.

The formation of molecular cation-anion π bonds is the essential element of a ferroelectric-type distortion in transition-metal oxides. I have pointed out elsewhere (6) how the energy gap between π and π^* bands of a linear chain of alternating cations and anions may be increased by a displacement δ of the cation subarray toward the anion subarray:

$$E_g = E_{g0} + A\delta + \dots \quad (6)$$

Since the number of bonding states stabilized by such a distortion is roughly proportional to E_g/W_b , where W_b is the total bandwidth of the $\pi + \pi^*$ bands, the total energy gain for the bonding π bands contains a term linear in δ that increases with E_{g0}/W_b . Where $1/2 < E_{g0}/W_b < 1$, the linear term may be large enough to produce a spontaneous, static crystallographic distortion at low temperatures. Such a distortion concentrates the occupied, bonding π electrons in the shorter V-O bonds.

Since π^* -orbital energies are destabilized by the distortion, the presence of π^* electrons after the distortion quenches the phenomenon. Therefore, these spontaneous, static distortions occur only where the destabilized π^* orbitals are empty after the distortion. In the case of VO₂, a ferroelectric-type, cooperative displacement of each vanadium ion toward an octahedral-site edge, so as to create an array of VO₂ clusters, would destabilize the two π^* bands relative to the $d_{||}$ band. These bands are emptied by the distortion, the electrons entering $d_{||}$ states. Furthermore, if the cation displacements along the c_r axis are antiparallel, so as to give an antiferroelectric distortion, then the c_r axis of the unit cell would be doubled and translational symmetry could split the $d_{||}$ band in two. Thus the \bar{d} -band configuration of Fig. 4 can be accomplished by an antiferroelectric distortion alone. However, the magnitude of the splitting of the $d_{||}$ band would be increased by simultaneous homopolar bonding between c_r -axis V-V pairs or by antiferromagnetic ordering of atomic spins induced by electron correlations.

The absence of antiferromagnetic order and the

structure (Fig. 2) of the monoclinic phase indicate that an antiferroelectric distortion is accompanied by V-V homopolar bonding in low-temperature ($T < T_i$) VO₂. The short V-O_I distance $R_{VO} = 1.76$ Å is characteristic of a single V-O π bond in addition to the σ bonding; the two V-O_{II} distances $R_{VO} = 1.86, 1.87$ Å are shorter than a bond having only σ bonding. Homopolar V-V bonding causes each vanadium to be nearly equidistant from the two bridging oxygens. Since each bridging oxygen shares its single p_π orbital between the two paired V⁴⁺ ions, an R_{VO} intermediate to that for a single π bond and that for no π bonding is anticipated.

Finally, formation of homopolar V-V bonding is most stable for a half-filled $d_{||}$ band, so this component of the distortion becomes energetically probable only after the π^* bands have been lifted above E_F , and hence at a $T_i' \leq T_i$. From this conclusion it also follows that the driving mechanism for the low-temperature distortion in VO₂ is the antiferroelectric component of the distortion, and the fact that $T_i' = T_i$ may be only a coincidence. With this model, the transition temperature T_i is controlled by the entropy of the lattice vibrational modes and not by the thermal excitation of electrons into the antibonding bands. Therefore, a $dT_i/dP > 0$ can be consistent with a $dE_g/dP < 0$.

A phase-diagram study at 1500°K (30) has shown that the rutile phase VO_{2+ ϵ} has a limited compositional range, $0.00 \leq \epsilon \leq 0.07$, and is always oxygen-rich. Since the majority carriers are holes, nonstoichiometric VO_{2+ ϵ} does not contain π^* electrons at $T < T_i$ to depress the transition temperature, and the T_i obtained by increasing temperature is only slightly decreased by $\epsilon > 0$ even though the discontinuity in electrical resistivity across the transition is reduced by several orders of magnitude. The T_i obtained by decreasing temperature, on the other hand, is considerably reduced, probably because lattice defects introduce energy barriers to the establishment of a long-range cooperative distortion. Kimizuka et al. (30) found that, in their crystals of VO_{2+ ϵ} , the T_i for rising temperature only decreases from 344°K at $\epsilon = 0.00$ to 336°K at $\epsilon = 0.07$, whereas the T_i for decreasing temperature is lowered to 295°K at $\epsilon = 0.07$. Ladd and Paul (2) had a thermal hysteresis as low as 1°K in their best samples, whereas it is larger than 40°K at $\epsilon = 0.07$. The discontinuity in the electrical resistance decreases from over four orders of magnitude at $\epsilon = 0.00$ to only a little more than one order of magnitude at $\epsilon = 0.07$.

The presence of two distinguishable components of the distortion in low-temperature VO₂ suggests

that the transition temperatures T_t and T_t' might be separated by the introduction of native defects, impurities, and/or hydrostatic pressure. Umeda et al. (31) were the first to report the observation of an intermediate phase in a small temperature interval $T_t' \leq T \leq T_t$ in samples of VO₂ containing about 1% titanium. Variations of T_t' and T_t with impurities and impurities plus native defects are discussed in Section IV. I am aware of no evidence for the separation of T_t and T_t' in pure VO_{2+ε} at atmospheric pressure, although Mitsubishi (32) has reported that crystals of V_{1-x}M_xO_{2+ε} grown from reagent grade V₂O₅ containing 100–500 ppm Al and 10–100 ppm Si impurities (M is Al and Si in concentrations $x \sim 0.002$) exhibit an intermediate phase in a temperature interval $T_t' \leq T \leq T_t$ that changes sensitively with ε. The possibility of separating T_t' and T_t with hydrostatic pressure would require an intermediate phase having a smaller volume than both the tetragonal and monoclinic phases. Although a discrepancy, according to the Clapeyron equation, has been reported between the volume change ΔV on going from the monoclinic to the

tetragonal phase, the entropy change (33), and the measured dT_t/dP (11), nevertheless dilatometric (34) and X-ray (35–38) measurements of the volume change ΔV across the transition are not consistent. The most recent measurement of ΔV (38) seems to eliminate any discrepancy with the Clapeyron equation that would suggest a dT_t/dP governed by a ΔV', the volume change on going from the tetragonal to an intermediate phase. The orthorhombic intermediate phase obtained by atomic substitution has a larger molecular volume and, therefore, should be suppressed by pressure.

IV. Mixed Systems

A number of workers have investigated the influence of cation substitutions on the transition temperature T_t and on the room-temperature structure. The results of these investigations are summarized in Table I. With the possible exceptions of Ge⁴⁺ and Ti⁴⁺, substitutional ions M³⁺ are unique in giving a $dT_t/dx > 0$ and an orthorhombic phase at room temperature if the impurity concentration

TABLE I

INITIAL RATE OF CHANGE OF UPPER TRANSITION TEMPERATURE WITH COMPOSITION (dT_t/dx) FOR THE SUBSTITUTIONAL COMPOUNDS V_{1-x}M_xO_{2+ε}, WHERE ε IS UNSPECIFIED AND PRESUMED ZERO

M	dT_t/dx [°K/at. % M]	x_1^a	x_2^a	$x_1 < x < x_2^a$	$x > x_2^a$	Refs.
Cr ³⁺	~+3	0.01	0.20	Orth.	(2φ) ^c	(16, 40–42)
Fe ³⁺	+3	0.01	0.125	Orth.	Two-phase	(32, 41–45)
Ga ³⁺	+6.5	0.005	0.02	Orth.	Two-phase	(46)
Al ³⁺	+9.0	0.005	0.045	Orth.	Two-phase	(32, 41, 42, 46)
Ti ⁴⁺	-0.5 to -0.7	0.2	0.2–0.25	Orth.	Rutile and (2φ) ^b	(16, 22, 32, 40, 45, 47–50)
Re ⁴⁺	~-4	0.07		Rutile		(47, 51)
Ir ⁴⁺	~-4	0.04	0.5	Rutile	Two-phase	(51)
Os ⁴⁺	-7	0.03	0.1	Rutile	Two-phase	(51)
Ru ⁴⁺	-10	0.025	0.75	Rutile	Two-phase	(51)
Ge ⁴⁺	+5					(32, 46, 52, 53)
Nb ⁵⁺	-7.8	0.05	0.9	Rutile	NbO ₂	(32, 41, 47, 54, 55)
Ta ⁵⁺	-5 to -10	0.02	0.5	Rutile	Two-phase	(45, 55)
Mo ⁶⁺	-5 to -10	0.03	0.55	Rutile	(2φ) ^b	(47, 56)
W ⁶⁺	-28	0.013	0.68	$x = 1.0$ Rutile	Mon. Orth.	(16, 57, 58)

Ordered trirutile phase about $x = 0.33$; $0.78 < x < 0.8$ (2φ)^b phase; $0.85 < x < 1$ mon.

^a Critical compositions x_1 and x_2 indicate phase changes at room temperature, and room-temperature structures within the regions $x_1 < x < x_2$ and $x > x_2$ are also indicated, where mon. refers to the monoclinic ($P2_1/c$) phase of Fig. 2 and orth. to the orthorhombic (probable space group $F222(39)$) phase of Fig. 5.

^b The 2φ phase is a distorted rutile structure with orthorhombic symmetry, and the 2φ' phase is similar but with monoclinic symmetry.

exceeds 1 at. %. A principal challenge to any model of the transition in VO_2 is to find an explanation for this phenomenon.

A recent study (41) of the phase diagram for the system $\text{V}_{1-x}\text{Cr}_x\text{O}_2$ traces two transition temperatures $T_i' \leq T_i$ in this system, the coincidence $T_i' = T_i$ occurring only in the limit $x \rightarrow 0$. At low chromium concentrations, the semiconductor-to-metal transition occurs at T_i where $dT_i/dx > 0$, and a semiconductor-to-semiconductor transition occurs at T_i' , where $dT_i'/dx < 0$ (31, 32). At higher x , the discontinuity $\Delta\rho$ in the resistivity across T_i or T_i' disappears. In the intermediate temperature range $T_i' < T < T_i$ the structure is orthorhombic. (Axes of unit cell are double those given in (41, 42). Triclinic cell of (32) is incorrect.) The structure is tetragonal (rutile) for $T > T_i$ and monoclinic (low-temperature VO_2) for $T < T_i'$.

A similar situation apparently occurs in all of the systems $\text{V}_{1-x}\text{M}_x\text{O}_2$. In the system $\text{V}_{1-x}\text{Fe}_x\text{O}_2$, Kosuge (43) observed two discontinuities in the magnetic susceptibility over the compositional range $0 < x \leq 0.04$, T_i' decreasing from 65 to 0°C and T_i increasing from 68 to 80°C. Mitsuishi (32) observed two discontinuities in the electrical resistivity vs temperature curve in samples containing $\text{M} = \text{Fe}$ ($x = 0.0012$ and 0.017), $\text{M} = \text{Cr}$ ($x = 0.0006$), $\text{M} = \text{Al}$ ($x = 0.0016$), and $\text{M} = \text{Ti}$ ($x = 0.045$), but not for $\text{M} = \text{Nb}$ ($x = 0.004$). In each case the semiconductor-to-metal transition occurs at the upper transition temperature T_i , a semiconductor-to-semiconductor transition at $T_i' < T_i$. The semiconducting energy gap is larger and the magnetic susceptibility smaller in the interval $T < T_i'$ than in the interval $T_i' < T < T_i$. These observations are

consistent with an antiferroelectric transition at T_i , the exchange-enhanced Pauli susceptibility disappearing with the Fermi surface on passing from a metallic to a semiconducting state, and the formation of V-V homopolar bonds below T_i' increasing the splitting of the $d_{||}$ band shown in Fig. 4. Mossbauer and NMR data on VO_2 containing 1 at. % titanium reveal that there is no antiferromagnetic ordering in either the monoclinic or the orthorhombic phases (31), which indicates spin-pairing in the $d_{||}$ band in both semiconducting phases.

The structure of the orthorhombic phase has not yet been refined. Figure 5 shows the relationship of the orthorhombic unit cell to the tetragonal (rutile) and monoclinic cells: $c_0 = a_m = 2c_r$ and $a_0 \approx b_0 \approx 2\sqrt{2}b_m = 2\sqrt{2}a_r$, $c_m = a_r - c_r$. This cell is large enough to accommodate an antiferroelectric displacement of the V^{4+} ions along the c_0 axis. Without homopolar V-V bonding along c_0 , each V^{4+} ion would form a close V-O bond with only one, instead of two, of its bridging oxygens to nearest-neighbor V^{4+} ions. The structure would then consist of VO_2 molecules (the $R_{\text{VO}} = 1.76 \text{ \AA}$ of the monoclinic phase also existing in the orthorhombic phase), and a nonuniform V-V spacing along $c_0 = 2c_r$ would split the $d_{||}$ band as required for a semiconducting phase. (See note added in proof at end of paper.)

With this model for the orthorhombic phase, it is now possible to interpret the findings summarized in Table I:

1. We should distinguish two components in the low-temperature distortion of VO_2 crystals to monoclinic symmetry: an antiferroelectric component and a V-V pairing along the $a_m = 2c_r$ axis,

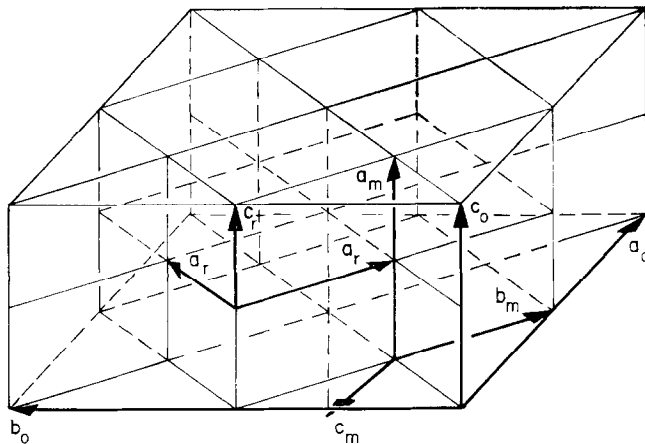


FIG. 5. Relationship of tetragonal and monoclinic phases to the orthorhombic phase of $\text{V}_{1-x}\text{M}_x\text{O}_2$, $\text{M} = \text{Al}, \text{Ga}, \text{Fe}, \text{Cr}, \text{Ti},$ or Ge .

the latter as a result of homopolar bonding via the single d electron per V⁴⁺ ion.

2. An antiferroelectric distortion is, in itself, capable of producing a semiconductor-to-metal transition. Such a distortion would raise the π^* bands of Fig. 3 above the Fermi energy E_F and simultaneously split the $d_{||}$ band in two, as shown in Fig. 4. However, the formation of V-V homopolar-bonded pairs along $a_m = 2c_r$ must increase the splitting of the $d_{||}$ band, thereby increasing the activation energy in the semiconducting state.

3. Since splitting of the $d_{||}$ band is energetically most favorable if the band is half-filled, the transition temperature for homopolar-bond formation is raised by the antiferroelectric component of the distortion, which raises the π^* bands above E_F . Therefore, if T_t is the transition temperature for the antiferroelectric component and T_t' is that for homopolar bonding, then the constraint $T_t' \leq T_t$ may be anticipated.

4. In pure, stoichiometric VO₂, the two transition temperatures coincide ($T_t' = T_t$), but cation substitutions V_{1-x}M_xO₂ may separate them. In any interval $T_t' < T < T_t$, a primarily antiferroelectric transition distorts the crystal to orthorhombic (probable space group $F222$) symmetry.

5. Substitution of foreign cations, which cannot participate in cooperative V-V homopolar bonding, necessarily decreases T_t' . From the system V_{1-x}Ti_x⁴⁺O₂, it appears that at $x = 0$ this decrease is

$$dT_t'/dx \lesssim -1^\circ\text{K/at.}\% \text{ impurity} \quad (7)$$

6. Addition of extra electrons to the vanadium d bands tends to introduce π^* electrons into the antiferroelectric state. Such electrons reduce the stabilization achieved by the antiferroelectric distortion, which increases the splitting between π and π^* bands, and, therefore, rapidly reduce T_t , making $dT_t/dx \ll 0$. The constraint $T_t' \leq T_t$ then keeps

$$dT_t'/dx = dT_t/dx \ll 0, \quad (8)$$

and there is only one crystallographic transition: monoclinic ($P2_1/c$) to tetragonal ($P4_2/mnm$). Furthermore, the resistivity of the distorted phase decreases with increasing x , and the discontinuity $\Delta\rho$ in the resistivity across T_t decreases sharply:

$$d(\Delta\rho)/dx \ll 0. \quad (9)$$

Extra electrons may be introduced into the vanadium d bands in two ways: (a) substitution of a higher valence-state cation, such as Nb⁵⁺, Ta⁵⁺, Mo⁶⁺, or W⁶⁺, and (b) substitution of a lower valence-state anion such as F⁻. These extra electrons may either be localized at discrete V³⁺ ions, as in

ordered, antiferromagnetic V₂³⁺W₆⁶⁺O₆ having the trirutile structure (58), or be mobile polarons. The systems V_{1-x}M_xO₂ having M = Nb, Ta, Mo, or W all show only a single transition from monoclinic to tetragonal symmetry that varies with x according to Eq. (8). They also show a rapid decrease in $\Delta\rho$ with increasing x as anticipated by Eq. (9).

Two studies of the system VO_{2-y}F_y have been made (59, 60). They found a $dT_t'/dy = dT_t/dy = -13$ to $-14^\circ\text{K/at.}\% \text{ F}^-$ and a rapid reduction with y in the resistance of the semiconducting phase. These data are both consistent with Eqs. (8) and (9), and hence with the addition of y electrons to the antibonding d bands of Fig. 4. In addition, the fact that dT_t'/dy for F⁻ additions has a larger magnitude than dT_t'/dx for Nb⁵⁺ or Ta⁵⁺ additions also supports the antiferroelectric hypothesis, since the more electronegative F⁻ ions do not form strong V-F π bonds and, therefore, do not contribute to stabilization of the cooperative antiferroelectric displacements. Both Nb⁵⁺ and Ta⁵⁺ ions may participate in these cooperative distortions.

7. Addition of delocalized holes to the semiconducting phase sharply reduces its resistivity and hence the discontinuity in resistivity $\Delta\rho$ across T_t , as already noted for the system VO_{2+ε}. Since the number of cation vacancies in VO_{2+ε} is $\epsilon/2$, it follows from Eq. (7) that

$$dT_t'/d(\epsilon/2) \approx -1^\circ\text{K/at.}\% \text{ cation vacancy}, \quad (10)$$

whereas a measured (30)

$$dT_t/d(\epsilon/2) = -2^\circ\text{K/at.}\% \text{ cation vacancy} \quad (11)$$

was found. Since the constraint $T_t' \leq T_t$ should hold, it follows that $dT_t'/d\epsilon = dT_t/d\epsilon$ in the system VO_{2+ε} and only one monoclinic-to-tetragonal transition is anticipated.

Not all of the holes introduced by a cation vacancy are itinerant. In fact probably three out of the four created by a cation vacancy must be trapped as discrete V⁵⁺ ions at cation sites nearest-neighbor to the vacancy. As discussed in paragraph 8 of this section, V⁵⁺ ions tend to stabilize an antiferroelectric distortion. If we assume one itinerant hole (three trapped holes) per cation vacancy and neglect the influence of cell size, it follows from Eq. (11) that

$$dT_t/d(\epsilon/2) \lesssim -2^\circ\text{K/at.}\% \text{ mobile holes}. \quad (12)$$

In the systems V_{1-x}M_x²⁺O₂, which have the formal valence formula V_{1-3x}V_{2x}³⁺M_x²⁺O₂, it is consistent to again assume one mobile hole (leaving one trapped hole) per M²⁺ ion. A $d(\Delta\rho)/dx \ll 0$ testifies to the existence of mobile holes. Since the ratio of localized holes (which increase T_t) to delocalized holes is

larger in $\text{VO}_{2+\epsilon}$ than in $\text{V}_{1-x}\text{M}_x^{2+}\text{O}_2$, by a factor 3, it follows that $dT_i/dx < -2^\circ\text{K/at.}\% \text{M}^{2+}$, in accord with a measured $dT_i/dx = -2$ to $-4^\circ\text{K/at.}\% \text{M}^{2+}$. From Eq. (7) and the constraint $T_i' < T_i$, this measured value gives $dT_i'/dx = dT_i/dx$, and a single monoclinic-to-tetragonal crystallographic distortion is predicted.

The resistivity of the monoclinic phase decreases rapidly with x (40), and the resistivity discontinuity $\Delta\rho$ across T_i has essentially disappeared for $x > 0.001$.

The fact that the thermal hysteresis is not markedly increased in the systems $\text{V}_{1-x}\text{M}_x^{2+}\text{O}_2$, in contrast to the system $\text{VO}_{2+\epsilon}$, supports the idea that a large thermal hysteresis is caused by an interruption of the long-range optical phonons by atomic vacancies.

8. Addition of localized holes, which create identifiable V^{5+} ions, enhances the stability of the antiferroelectric distortion, since V^{5+} ions are not stable in an oxygen octahedron. Because V^{5+} ions are small and have empty d orbitals available for π bonding, they are always displaced from the center of an octahedral interstice so as to reduce the anion coordination. Similarly small cations having no outer electrons in partially filled d shells, such as Al^{3+} , Ga^{3+} , and Ge^{4+} (the Si^{4+} ion is too small to enter an octahedral site at atmospheric pressure (40)), stabilize the antiferroelectric distortion, since they are more stable in a smaller anion coordination.

In the substitutional system $\text{V}_{1-2x}^{4+}\text{V}_x^{5+}\text{M}_x^{3+}\text{O}_2$, all the d holes (one per M^{3+} ion) appear to be trapped as discrete V^{5+} ions at cation sites nearest-neighbor to the M^{3+} ions. This permits a $dT_i/dx > 0$ since there are no itinerant holes left over. Therefore, in these systems

$$dT_i/dx > 0 > dT_i'/dx \quad (13)$$

and an orthorhombic, semiconducting phase appears in the interval $T_i' < T < T_i$. The fact that dT_i/dx is largest for $\text{M} = \text{Al}$ is consistent with the small size of the Al^{3+} ion. The Cr^{3+} ion, on the other hand, has a pronounced octahedral-site preference energy, so dT_i/dx is expected to be smallest for $\text{M} = \text{Cr}$.

$\text{V}_{1-x}\text{M}_x\text{O}_2$ crystals containing $\text{M} = \text{Al}$ or Cr exhibit

$$d(\Delta\rho)/dx < 0, \quad (14)$$

as in the previous systems discussed (40). However, these systems differ by retaining a large resistivity below T_i , the decrease in $\Delta\rho$ occurring because of a marked increase in the resistivity of the tetragonal phase. Above T_i , the temperature coefficient of the resistivity is changed from metallic to semiconducting, indicating a sharp decrease in the electron

mobilities of the high-temperature phase. This observation is consistent with the creation of discrete V^{5+} ions trapped at M^{3+} -ion centers: noncooperative displacements of the V^{5+} ions to form shorter $\text{V}-\text{O}$ bonds would perturb the narrow π^* bands, thereby narrowing them and tending to lift the bottom of the π^* bands above E_F . If this occurs, conductivity would be primarily in the narrower $d_{||}$ bands. A temperature-dependent magnetic susceptibility signals exchange enhancement due to $d_{||}$ electrons, so low $d_{||}$ -electron mobilities, if not exchange splitting of the $d_{||}$ band, are anticipated.

9. The Ti^{4+} ion is not small enough to contribute spontaneously to the antiferroelectric distortion in VO_2 (TiO_2 is not distorted), but it readily participates in this distortion (BaTiO_3 exhibits ferroelectric distortions) since it has empty $3d$ orbitals to participate in π bonding. This reasoning is consistent with a

$$dT_i/dx \approx -0.5 \text{ to } -0.7^\circ\text{K/at.}\% \text{Ti}^{4+} \quad (15)$$

that is markedly smaller in magnitude than the $dT_i/dx < 0$ found for substitutions of Re^{4+} , Ir^{4+} , Os^{4+} , or Ru^{4+} ions, since the ions having partially filled d shells cannot participate in the antiferroelectric distortion. Comparison of Eqs. (7) and (15) shows a $dT_i'/dx < dT_i/dx$ in $\text{V}_{1-x}\text{Ti}_x\text{O}_2$, and an orthorhombic phase appears in the interval $T_i' < T < T_i$.

$\text{V}_{1-x}\text{Ti}_x\text{O}_2$ also shows a $d(\Delta\rho)/dx < 0$ as a result of a sharp increase in the resistivity of the high-temperature phase, the resistivity of the low-temperature phase showing little change. Since the d bands of TiO_2 are at 3.05 eV above the top of the π band, whereas E_F is about 2.5 eV above this band in VO_2 , the $3d$ orbitals of a Ti^{4+} ion form deep acceptor levels. This change in the d -electron potential, as in the case of discrete V^{5+} ions trapped at M^{3+} -ion centers, would perturb the π^* bands and allow for a sharp decrease in the electron mobilities of the high-temperature phase.

V. Final Remarks

The appearance of two transition temperatures, T_i' and T_i , in cation-substituted VO_2 is to be distinguished from the appearance of two transitions in the Magnéli ($6J$) phases $\text{Ti}_n\text{O}_{2n-1}$ and $\text{V}_n\text{O}_{2n-1}$. In this latter case, the two transitions probably represent the coexistence of two adjacent Magnéli phases, each with a different n . Figure 6 illustrates magnetic-susceptibility data of Vasil'ev and Ariya (62) for different values of x in the system TiO_x . The values

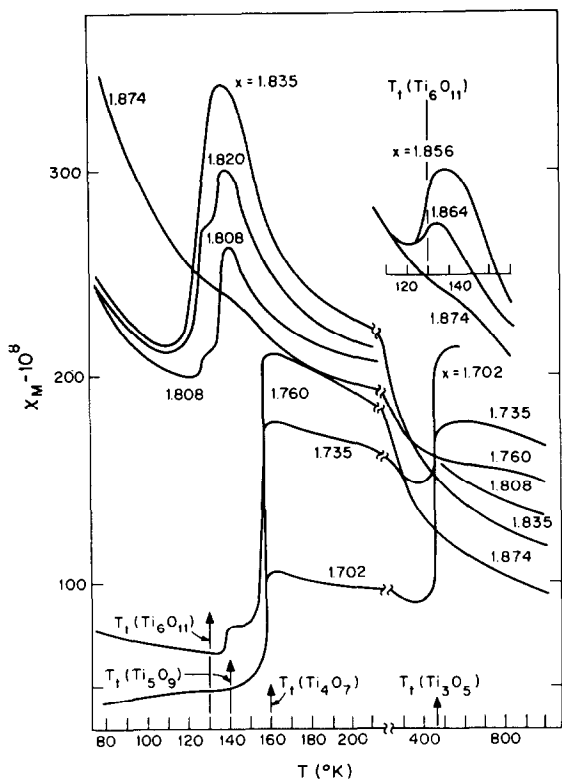


FIG. 6. Magnetic susceptibility versus temperature of TiO_x for several values of x . Data from Ref. (62).

$x = 1.67, 1.75, 1.80, 1.833, 1.857,$ and 1.875 correspond to $n = 3-8$ in the series Ti_{*n*}O_{2*n*-1}. The Magnéli phases have $n \geq 4$, and transition temperatures for Ti₃O₅, Ti₄O₇, Ti₅O₉, and Ti₆O₁₁ can be distinguished in the figure. It is clear that two transition temperatures are observed where the crystal is not single phase. Pure phases exhibiting a single transition temperature have been reported by Mulay and Danley (63). This point is emphasized because of a recent speculation (38) that the appearance of two transition temperatures in what was presumed to be single-phase Magnéli structures is related to the appearance of two transition temperatures in impure VO₂ samples.

One point of similarity between the Magnéli phases and VO₂ may be argued (64). In the Magnéli phases, rutile slabs are connected by shear planes across which cations share common octahedral-site faces. At high temperatures, the cation-cation separations across these planes are relatively large, indicating that ferroelectric-type displacements (in cooperation with electrostatic forces) destabilize the π^* orbitals at the shear planes. Consequently the d electrons are itinerant within the rutile slabs, according to Fig. 3, and tunneling across the shear

planes renders the phases metallic. At low temperatures ($T < T_t$), electrons in the Ti_{*n*}O_{2*n*-1} phases could be trapped by homopolar-bond formation across the shear planes: such homopolar bonding would just trap all of the d electrons, rendering the phase semiconducting (6). In the V_{*n*}O_{2*n*-1} phases, such trapping must also be accompanied by an antiferroelectric distortion within the rutile blocks if semiconducting properties are to occur.

Several other compounds, including MoO₂ and WO₂, appear to be isostructural with low-temperature VO₂. However, a review of the structure refinements for these phases (65) indicates that there is no shortest M-O bond perpendicular to the $a_m = 2c$, axis. In these compounds the shortest M-O separations are to the bridging oxygens between M-M pairs. This observation shows that the antiferroelectric component of the distortion is suppressed, as it should be because the one more d electron per M⁴⁺ cation must occupy π^* orbitals. In fact, these π^* electrons must be the charge carriers in these metals, since the $d_{||}$ electrons are tied up in homopolar M-M bonds. In compounds where an antiferroelectric distortion cannot occur, the constraint $T_t' \leq T_t$ cannot hold. In systems V_{1-x}M_xO₂, there are sufficient like cations for cooperative M-M homopolar bonding to occur as $x \rightarrow 1.0$, and a $T_t' > 0$ may reappear at large x without any antiferroelectric component to the distortion. However, the constraint $T_t' \leq T_t$ should hold for small x .

A structural refinement of orthorhombic V_{1-x}M_x³⁺O₂ would establish the antiferroelectric hypothesis, and this refinement is now in progress.

Note Added in Proof: A structure refinement of the orthorhombic phase of V_{0.95}Cr_{0.05}O₂ by J. W. Pierce indicates that the probable space group is F222 and the room-temperature lattice parameters are $a_0 = 13.015\text{\AA}$, $b_0 = 12.597\text{\AA}$, $c_0 = 5.795\text{\AA}$. The structure contains four distinguishable c -axis chains of edge-shared octahedra: Cations V₁ in 4a and V₂ in 4b occupy alternate positions of one chain, the V₁-O separations being nearly uniform ($\approx 1.895\text{\AA}$) whereas the V₂-O distances along b_0 are shorter (1.85\AA) and the four others are longer (2.04\AA). Cations V₃ in 8j and V₄ in 8i exhibit antiferroelectric displacements along half the c -axis chains, and cations V₅ form V₅-V₅ pairs along the fourth c -axis chain. Although this structure is more complex than anticipated, it exhibits all the essential features: V-V c -axis pairs are reduced to 1/4 their concentration in the monoclinic phase, the c -axis is doubled, and all but one of the d_{π} orbitals (a d_{yz} orbital of V₂) is destabilized by increased covalent mixing with the anions.

Acknowledgment

I wish to express my sincere thanks to B. L. Chamberland for communicating his compilation of data on the cation-substituted systems. These data are summarized in Table I.

References

1. F. J. MORIN, *Phys. Rev. Lett.* **3**, 34 (1959).
2. L. A. LADD AND W. PAUL, *Solid State Commun.* **7**, 425 (1969).
3. A. MAGNÉLI AND G. ANDERSSON, *Acta Chem. Scand.* **9**, 1378 (1955); A. MAGNÉLI, *Acta Crystallogr.* **9**, 1038 (1956).
4. J. B. GOODENOUGH, *Phys. Rev.* **117**, 1442 (1960).
5. J. B. GOODENOUGH, Colloques Internationaux du CNRS No. 157, *Propriétés Thermodynamiques Physiques et Structurales des Dérivés Semi-Métalliques*, p. 263. Orsay, 28 Sept.-1 Oct. 1965, Editions CNRS, Paris, 1967.
6. J. B. GOODENOUGH, *Czech. J. Phys. B* **17**, 304 (1967).
7. D. ADLER AND H. BROOKS, *Phys. Rev.* **155**, 826 (1967).
8. A. S. BARKER, JR., H. W. VERLEUR, AND H. J. GUGGENHEIM, *Phys. Rev. Lett.* **17**, 1286 (1966).
9. S. KOIDE AND H. TAKEI, *J. Phys. Soc. Jap.* **22**, 946 (1967).
10. H. W. VERLEUR, A. S. BARKER, JR., AND C. N. BERGLUND, *Phys. Rev.* **172**, 788 (1968).
11. C. N. BERGLUND AND A. JAYARAMAN, *Phys. Rev.* **185**, 1034 (1969).
12. R. HECKINGBOTTOM AND J. W. LINETT, *Nature (London)* **194** 678 (1962).
13. J. B. GOODENOUGH AND J. M. LONGO, Landolt-Bornstein Tabellen Neue Serie III/4a, p. 126. Springer-Verlag, Berlin, 1970.
14. J. B. GOODENOUGH, *Phys. Rev.* **164**, 785 (1967).
15. K. V. KRISHNA RAO, S. V. NAGENDER NAIDU, AND L. IYENGAR, *J. Phys. Soc. Jap.* **23**, 1380 (1967).
16. M. ISRAELSSON AND L. KIHLBORG, *Mater. Res. Bull.* **5**, 19 (1970).
17. P. F. BONGERS, *Solid State Commun.* **3**, 275 (1965).
18. K. KOSUGE, *J. Phys. Soc. Jap.* **22**, 551 (1967).
19. M. CARDONA AND G. HARBEKE, *Phys. Rev. A* **137**, 1467 (1965).
20. J. B. GOODENOUGH, *J. Phys. Chem. Solids* **30**, 261 (1969).
21. R. J. POWELL, C. N. BERGLUND, AND W. E. SPICER, *Phys. Rev.* **178**, 1410 (1969).
22. W. RÜDORFF, G. WALTER, AND J. STADLER, *Z. Anorg. Allg. Chem.* **297**, 1 (1958).
24. J. UMEDA, H. KUSUMOTO, K. NARITA, AND E. YAMADA, *J. Chem. Phys.* **42**, 1458 (1965); *J. Phys. Soc. Jap.* **21**, Suppl. XV-2, 619 (1966).
24. K. KOSUGE, *J. Phys. Soc. Jap.* **22**, 551 (1967).
25. A. D. WADSLY, *Acta Crystallogr.* **8**, 695 (1955).
26. J. GALY, J. DARRIET, A. CASALOT, AND J. B. GOODENOUGH, *J. Solid State Chem.* **1**, 339 (1970).
27. K. A. WILHELMI, K. WALTERSSON, AND L. KIHLBORG, private communication.
28. J. B. GOODENOUGH, *J. Solid State Chem.* **1**, 349 (1970).
29. J. B. GOODENOUGH, "Int. Conf. on Conduction in Low Mobility Materials," Eilat, Israel, April 5-8, 1971: To be published in *Adv. in Physics, Suppl. London*.
30. N. KIMIZUKA, M. SAEKI, AND M. NAKAHIRA, *Mater. Res. Bull.* **5**, 403 (1970).
31. J. UMEDA, S. ASHIDA, H. KUSUMOTO, AND K. NARITA, *J. Phys. Soc. Jap.* **21**, 1461 (1966).
32. T. MITSUISHI, *Jap. J. Appl. Phys.* **6**, 1060 (1967).
33. E. RYDER, quoted in Ref. (37).
34. T. KAWAKUBO AND T. NAKAGAWA, *J. Phys. Soc. Jap.* **19**, 517 (1964).
35. S. MINOMURA AND H. NAGASAKI, *J. Phys. Soc. Jap.* **19**, 131 (1964).
36. J. M. LONGO AND P. KIERKEGAARD, *Acta Chem. Scand.* **24**, 420 (1970).
37. SVEN WESTMAN, *Acta Chem. Scand.* **15**, 217 (1961).
38. M. MAREZIO, P. D. DERNIER, D. B. MCWHAN, AND J. P. REMEIKA, *Mater. Res. Bull.* **5**, 1015 (1970).
39. J. W. PIERCE, private communication.
40. J. B. MACCHESNEY AND H. J. GUGGENHEIM, *J. Phys. Chem. Solids* **30**, 225 (1969).
41. G. VILLENEUVE, A. BORDET, A. CASALOT, AND P. HAGENMULLER, *Mater. Res. Bull.* **6**, 119 (1971).
42. J. GALY, A. CASALOT, AND P. HAGENMULLER, *Bull. Soc. Chim. Fr.*, 227 (1967).
43. K. KOSUGE, *J. Phys. Soc. Jap.* **22**, 551 (1967).
44. C. R. EVERHART AND J. B. MACCHESNEY, *J. Appl. Phys.* **39**, 2872 (1968).
45. U.S. patent 3,402,131, Sept. 17, 1968.
46. I. KITAHIRO AND A. WATANABE, *Jap. J. Appl. Phys.* **6**, 1023 (1967).
47. B.-O. MARINDER AND A. MAGNÉLI, *Acta Chem. Scand.* **11**, 1635 (1957); **12**, 1345 (1958).
48. L. K. KRISTENSEN, *J. Appl. Phys.* **39**, 5341 (1968).
49. S. M. ARIYA AND G. GROSSMAN, *Sov. Phys.-Solid State* **2**, 1166 (1960).
50. B.-O. MARINDER AND S. FRIBERG in A. Magnéli et al., Univ. of Stockholm Final Technical Report [DA-91-591-EUC-1319] (1960).
51. B. L. CHAMBERLAND AND D. B. ROGERS, U.S. patent 3,542,697, Nov. 24, 1970.
52. M. AOHI, K. KABAYASHI, AND H. FUTUKI, Abstract of the Fall Meeting of the Appl. Phys. Soc. Jap. **59** (1965).
53. C. H. NEUMAN, A. W. LAWSON, AND R. F. BROWN, *J. Chem. Phys.* **41**, 1591 (1964).
54. W. RÜDORFF AND J. MÄRKLIN, *Z. Anorg. Allg. Chem.* **334**, 142 (1964).
55. H. TRARIEUX, J. C. BERNIER, AND A. MICHEL, *Ann. Chim. (Paris)* **4**, 183 (1969).
56. L. KIHLBORG in P. Kierkegaard, S. Axrup, M. Israelsson, G. Barrling, L. Kihlborg, K. Eistrat, A. Kopwillem, L.-O. Hagman, B. Linnros, and M. Seleborg, Univ. Stockholm, *Inorg. Phys. Chem.*, DIS No. 31.
57. M. NYGREN AND M. ISRAELSSON, *Mater. Res. Bull.* **4**, 881 (1961).
58. W. RÜDORFF AND H. KORNELSON, *Angew. Chem., Int. Ed. Engl.* **7**, 229 (1968).
59. B. L. CHAMBERLAND, U.S. patent 3,532,641, Oct. 6, 1970; *Mater. Res. Bull.* (in press).
60. T. G. REYNOLDS, M. L. F. BAYARD, M. VLASSE, H. L. MCKINZIE, R. J. ARNOTT, AND A. WOLD, *J. Solid State Chem.* **3**, 484 (1971).
61. A. MAGNÉLI, *Nature (London)* **115**, 356 (1950); *Ark. Kemi* **1**, 513 (1950).
62. YA. V. VASIL'EV AND S. M. ARIYA, *Izv. Akad. Nauk SSSR, Neorg. Mater.* **1**, 347 (1965); *Inorg. Mater. (USSR)* **1**, 322 (1965).
63. L. N. MULAY AND W. J. DANLEY, *J. Appl. Phys.* **41**, 877 (1970).
64. J. B. GOODENOUGH, *Progr. Solid State Chem.* **5**, in press.
65. A. MAGNÉLI, *Ark. Kemi, Mineral. Geol. A* **24** (1946).